First Direct Measurement of Sub-Nanosecond Polarization Switching in Ferroelectric Hafnium Zirconium Oxide

X. Lyu[1], M. Si[1], P. R. Shrestha[2], K. P. Cheung[2] and P. D. Ye[1,*]
[1]School of Electrical and Computer Engineering, Purdue University, West Lafayette, USA, *email: yep@purdue.edu
[2]National Institute of Standards and Technology, Gaithersburg, USA

***Abstract*—**In this work, we report on an ultrafast direct measurement on the transient ferroelectric polarization switching in hafnium zirconium oxide with a crossbar metal-insulator-metal (MIM) structure. A record low sub-nanosecond characteristic switching time of 925 ps was achieved, supported by the nucleation limited switching model. The impact of electric field, film thickness and device area on the polarization switching speed is systematically studied.

I. Introduction

Due to the fast speed [1-7], high retention/endurance [8, 9] and CMOS compatible process, ferroelectric (FE) hafnium oxide (HfO_2), such as hafnium zirconium oxide (HZO) [10], has been the promising material for various ferroelectric device applications such as ferroelectric memory (FeRAM), ferroelectric field-effect transistors (Fe-FETs) [1,2,4] and negative-capacitance FETs (NC-FETs) [11-13]. In all these devices, ferroelectric polarization switching speed is a critical factor, which directly determines the working speed of the device. The reported ferroelectric polarization switching times in literatures broadly scatter from few ns to μs [1-7]. Recently, it was studied that the RC time constant in the measurement system can be one of the key problems to under-estimate the intrinsic fast switch speed of ferroelectric hafnium oxide, leading to a broad distribution of polarization switching time [7]. By excluding the impact of RC, 10 ns full polarization switching or few ns characteristics switching time (t_0) were achieved [7]. The fast, scalable in dimension and non-volatile properties enable HfO_2 based Fe-FET to be a strong energy-efficient candidate for non-volatile memory applications and even for the faster volatile memories [14]. However, to replace volatile memories like dynamic RAM (DRAM) or even static RAM (SRAM), sub-ns or GHz operational speed is required and has not been demonstrated in FE HfO_2 system directly.

In this work, the transient ferroelectric polarization switching dynamics in HZO is directly measured by an ultrafast pulse measurement setup. A record low characteristic switching time down to 925 ps is achieved for the first time in sub-ns range, extracted by a nucleation limited switching (NLS) model [15]. A W/HZO/W crossbar capacitor structure and fabrication process are developed to scale down the device area to few μm^2. RC time constants are carefully measured by both capacitance and resistance measurements directly. It is demonstrated that the capacitor area has a significant impact on polarization switching time not because of the RC time constant but due to the intrinsic area dependence. The intrinsic area dependence is ascribed to the multi-grain polycrystalline nature of the FE HZO thin film. The electric field dependence and film thickness dependence are also systematically studied.

II. Experiments

A photo image of the fabricated W/HZO/W crossbar MIM structure is shown in Fig. 1. W is used for both top and bottom electrodes. Ti/Au pad is used on top of bottom W electrode to prevent HZO thin film formation during the atomic layer deposition (ALD) process and also reduce the probe contact resistance. An insulating sapphire substrate is employed to reduce the parasitic effects and signal reflection. The device fabrication process is described in Fig. 2(a). The starting point is an insulating sapphire substrate. W sputtering followed by CF_4/Ar dry etch was used to pattern the bottom W electrodes. Ti/Au contact pads were then defined by photo lithography, e-beam evaporation and a lift-off process. HZO (Hf:Zr=1:1) was deposited by ALD at 200 °C using TDMAHf ($[(CH_3)_2N]_4Hf$), TDMAZr ($[(CH_3)_2N]_4Zr$) and H_2O as Hf, Zr and O precursors. The top W electrodes were defined by sputtering and a lift-off process. A 500 °C rapid thermal annealing was then performed in N_2 for 60 s. Fig. 2(b) and 2(c) shows the cross-sectional schematic of fabricated capacitor and the TEM image on FE HZO. Fig. 3 shows the polarization versus electric field (P-E) hysteresis loop of a crossbar MIM capacitor with 8 nm HZO, showing well-behaved ferroelectric properties. Fig. 4 shows the capacitance-voltage (C-V) characteristics of a crossbar MIM capacitor with 15 nm HZO, with a typical butterfly-shape ferroelectric hysteresis. Fig. 5 is a circuit diagram of the ultrafast pulse measurement setup. A high speed pulse generator along with high speed and high power amplifier (leading to maximum of ~9 V and 300 ps rise time in this work) and a 80 GS/s oscilloscope were used to generate the voltage pulses and monitor the transient switching current. Impedance matched probes and pick-off tee were used to minimize the signal reflections. A positive-up-negative-down (PUND) pulse sequence was applied to directly measure the polarization switching current [7, 16], as shown in Fig. 6, highlighting the preset pulse, switching pulse and non-switching pulse, as also pointed out in Fig. 3. Fig. 7 shows the resistances and the corresponding RC time constant versus different areas, among which the smallest RC constant is below 200 ps. The RC time constants are calculated using experimentally measured resistances and capacitances.

III. Results and Discussion

The voltage pulses with 300 ps rise-time and the corresponding transient current responses are shown in Fig. 8 for both switching (pulse 1) and non-switching (pulse 2) pulses in the PUND measurement. The current response to switching pulse

(I_{pulse1}) is wider compared to the current response to non-switching pulse (I_{pulse2}) due to the extra polarization switching current. Fig. 9 plots the transient current I_{pulse1}, I_{pulse2} and I_{FE} in the same time scale. The net polarization switching current I_{FE} is calculated by $I_{FE}=I_{pulse1}-I_{pulse2}$. The transient polarization charge density is calculated by the integration of I_{FE} ($P = \int I_{FE}\, dt$), as shown in Fig. 10. A nucleation limited switching model was applied for the multi-grain polycrystalline HZO to extract the characteristic switching time constant. In NLS model for a single grain element, the polarization switching dynamics follow the equation as $P = P_S(1 - \exp(-\left(\frac{t}{t_0}\right)^{\beta}))$, where β is an exponential parameter and t_0 is a voltage-dependent characteristic switching time [5,15]. β=2 is used in this work due to 2-dimentional nature of thin film. Sub-ns polarization switching was achieved in 15 nm HZO at 9 V and with a device area of 8.4 μm^2, where the extracted characteristic switching time is 925 ps, as shown in Fig. 10.

The transient FE switching currents for 15 nm HZO capacitors with different areas (Voltage=9 V, E=0.6 V/nm) are plotted in Fig. 11 and the corresponding transient polarization charge densities are shown in Fig. 12. There is a clear area-dependent switching speed as indicated in Fig. 13. The RC time constants for these devices (as shown in Fig. 7) are about 5 times smaller than the characteristic switching times, suggesting the measured switching speed is not limited by the RC effect. Therefore, the ferroelectric polarization switching has an intrinsic area dependence. It is understood that the polarization switching process in polycrystalline FE thin film is a sequential switching process of each elemental grain, according to the nucleation limited switching model, as shown in Fig. 14. At scaled device size, the grain number is significantly reduced so that the polarization switching speed is improved.

Measurements of I_{FE} on 10 nm HZO capacitors under different electric fields are shown in Fig. 15, showing a clear electric field dependence. The corresponding transient polarization charge densities are shown in Fig. 16. Fig. 17 shows the extracted characteristic switching time versus electric field for 10 nm HZO, showing faster polarization switching under higher electric field. Fig. 18 and Fig. 19 show the thickness-dependent transient polarization switching current and transient polarization charge density. The HZO capacitors of each thickness are measured at maximum voltage allowed. The corresponding extracted characteristic time constants versus HZO thickness is shown in Fig. 20, from which the trend of thickness dependence is clear that thicker films are faster. Fig. 21 is a summary of the thickness-dependent remnant polarization (P_r).

The ferroelectric polarization switching time of the FE HZO crossbar capacitor is benchmarked with the reported fastest polarization switching times on FE HfO_2 in literatures, as shown in Table. I. The experimental devices have different structures including capacitor structure (MIM) and FeFET structure, different FE HfO_2, different electrode materials including W, WN, TiN and Ni, different thicknesses from 8 nm to 15 nm and different applied voltage so that under different electric fields. Fig. 22 shows the switching time versus electric field from the benchmark Table I. In this work, a sub-ns (925 ps) record low full polarization switching time is achieved for the first time.

IV. Conclusion

In summary, we report on a record low sub-ns characteristic switching time of 925 ps on FE HZO, by a direct ultrafast measurement of transient polarization switching current. The impact of electric field, film thickness and device area on polarization switching speed is systematically studied. The ferroelectric switching speed is significantly improved compared to previous reports and more importantly is approaching GHz regime, suggesting FE HZO to be a promising and competitive high-speed non-volatile memory technology and has the potential even to replace the DRAM and SRAM for high-density, high-speed, and both on-chip and off-chip memories.

Acknowledgment

The authors gratefully acknowledge valuable discussions from J. P. Campbell and S. Salahuddin, technical support from X. Sun and H. Wang on TEM imaging, and the funding support from DARPA/SRC JUMP ASCENT Center.

References

[1] W. Chung *et al.*, "First Direct Experimental Studies of $Hf_{0.5}Zr_{0.5}O_2$ Ferroelectric Polarization Switching Down to 100-picosecond in Sub-60mV/dec Germanium Ferroelectric Nanowire FETs," *IEEE Symposium on VLSI*, pp. T89-T90, 2018.

[2] E. Yurchuk *et al.*, "Impact of Scaling on the Performance of HfO_2-Based Ferroelectric Field Effect Transistors," *IEEE Trans. Electron Devices*, vol. 61, pp. 3699-3706, 2014.

[3] H. K. Yoo *et al.*, "Engineering of Ferroelectric Switching Speed in Si Doped HfO_2 for High-Speed 1T-FERAM Application," *IEEE International Electron Devices Meeting*, pp. 481-484, 2017.

[4] S. Dunkel *et al.*, "A FeFET based super-low-power ultra-fast embedded NVM technology for 22nm FDSOI and beyond," *IEEE International Electron Devices Meeting*, pp. 485-488, 2017.

[5] C. Alessandri *et al.*, "Switching Dynamics of Ferroelectric Zr-Doped HfO_2," *IEEE Electron Device Lett*, vol. 39, pp. 1780-1783, 2018.

[6] X. Lyu *et al.*, "Ferroelectric and Anti-Ferroelectric Hafnium Zirconium Oxide: Scaling Limit, Switching Speed and Record High Polarization Density," *IEEE Symposium on VLSI*, pp. T89-T90, 2019.

[7] M. Si et al., "Ultrafast Measurements of Polarization Switching Dynamics on Ferroelectric and Anti-Ferroelectric Hafnium Zirconium Oxide," *Appl. Phys. Lett.* (under review), 2019.

[8] N. Gong *et al.*, "Why is FE–HfO_2 more suitable than PZT or SBT for scaled nonvolatile 1-T memory cell? A retention perspective," *IEEE Electron Device Lett*, vol. 37, pp. 1123-1126, 2016.

[9] K. Ni *et al.*, "Critical role of interlayer in $Hf_{0.5}Zr_{0.5}O_2$ ferroelectric FET nonvolatile memory performance," *IEEE Trans. Electron Devices*, vol. 65, pp 2461-2469, 2018.

[10] J. Muller *et al.*, "Ferroelectricity in Simple Binary ZrO_2 and HfO_2," *Nano Lett.*, vol. 12, pp.4318-4323, 2012.

[11] S. Salahuddin *et al.*, "Use of negative capacitance to provide voltage amplification for low power nanoscale devices," *Nano Lett.*, vol. 8, pp. 405-410, 2008.

[12] M. Si *et al.*, "Steep-slope hysteresis-free negative capacitance MoS_2 transistors," *Nat. Nanotechnol.*, vol. 13, pp. 24-28, 2018.

[13] M. A. Alam *et al.*, "A critical review of recent progress on negative capacitance field-effect transistors", *Appl. Phys. Lett.*, vol. 114, p. 090401, 2019.

[14] K.-H. Kim *et al.*, "Ferroelectric DRAM (FEDRAM) FET with metal/$SrBi_2Ta_2O_9$/SiN/Si gate structure", *IEEE Electron Device Lett.*, vol. 23, pp 82-84, 2002.

[15] J. Y. Jo *et al.*, "Domain switching kinetics in disordered ferroelectric thin films," *Phys. Rev. Lett.*, vol. 99, p. 267602, 2007.

[16] A. Grigoriev *et al.*, "Ultrafast electrical measurements of polarization dynamics in ferroelectric thin-film capacitors," *Rev. Sci. Instrum.*, vol. 80, p. 124704, 2011.

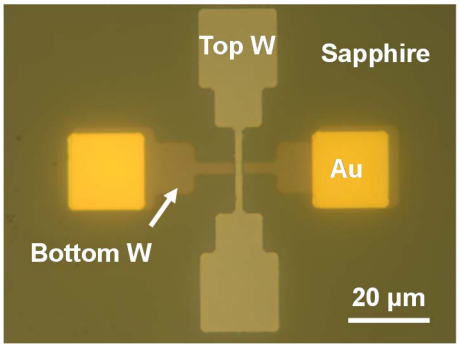

Fig. 1. Photo image of a W/HZO/W crossbar capacitor. An insulator sapphire substrate is used to minimize parasitic capacitance and signal reflection.

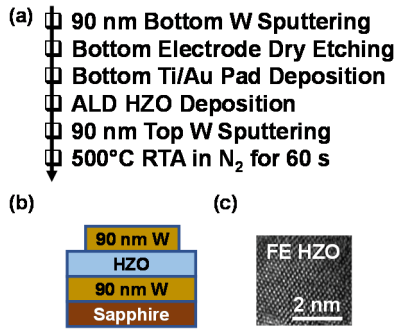

Fig. 2. (a) Device fabrication process flow. (b) Cross-sectional schematic diagram and (c) TEM image of FE HZO.

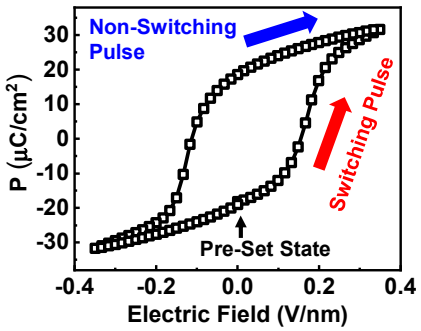

Fig. 3. P-E characteristics of a representative capacitor with 8 nm HZO.

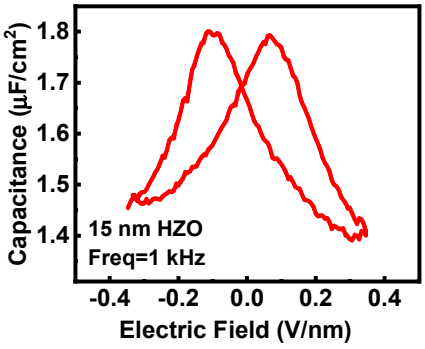

Fig. 4. C-V characteristics of a representative capacitor with 15 nm HZO.

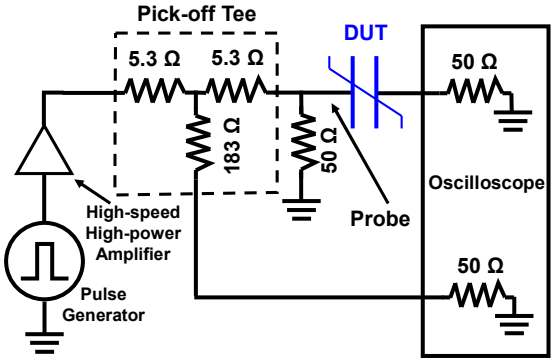

Fig. 5. Circuit diagram of the ultrafast pulse measurement setup with a pulse rise time of ~300 ps.

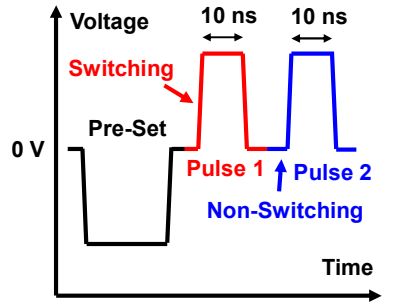

Fig. 6. PUND pulse sequence for transient ferroelectric polarization switching measurement.

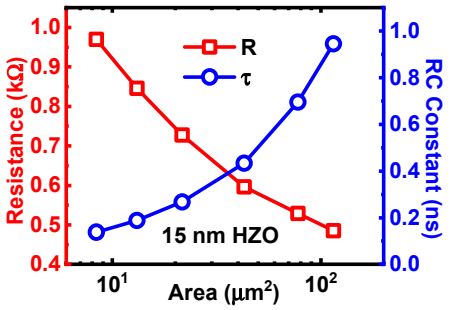

Fig. 7. Resistances and RC time constants of 15 nm HZO MIM devices. RC time constant below 200 ps is achieved and does not affect the speed measurements.

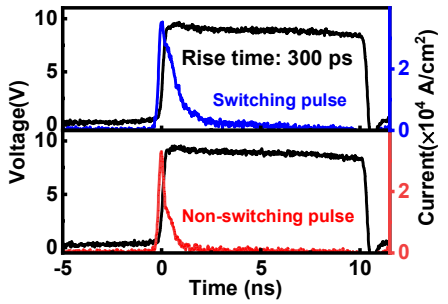

Fig. 8. 10 ns ultrafast pulse input with a 300 ps rise time and the transient current response of the switching (pulse 1) and non-switching (pulse 2) pulses.

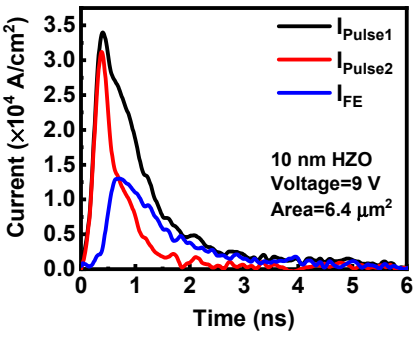

Fig. 9. Transient current I_{pulse1}, I_{pulse2} and I_{FE} of a 10 nm HZO capacitor.

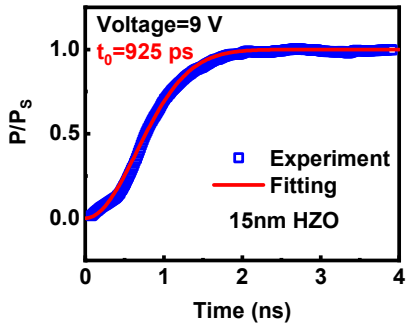

Fig. 10. Normalized transient switched polarization charge density from both experiment and fitting by NLS model. Characteristic switching time is achieved to be 925 ps.

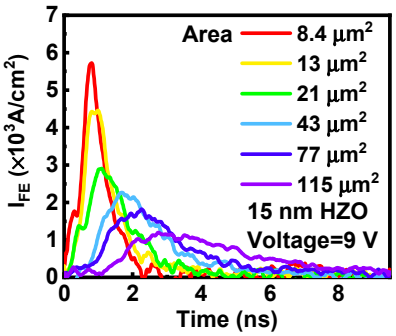

Fig. 11. Transient polarization switching current of 15 nm HZO capacitors with different areas.

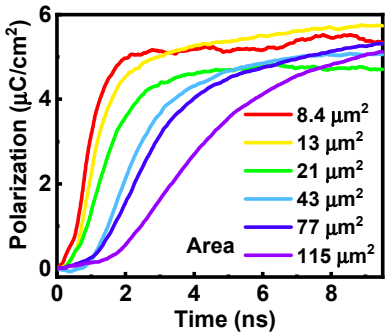

Fig. 12. The corresponding transient polarization charge density by the integration of I_{FE} over time in Fig. 11.

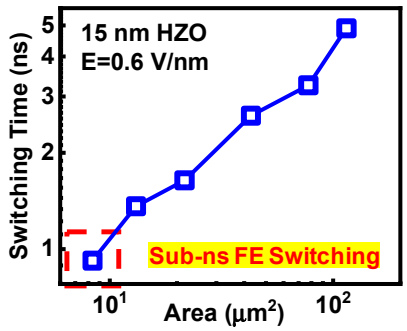

Fig. 13. Area-dependent characteristic switching time in 15 nm HZO.

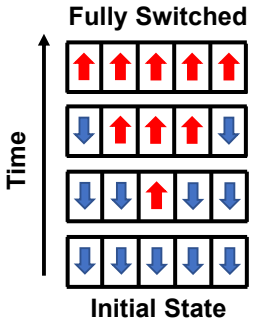

Fig. 14. Illustration of the impact of polycrystalline multi-grains on the FE polarization switching process.

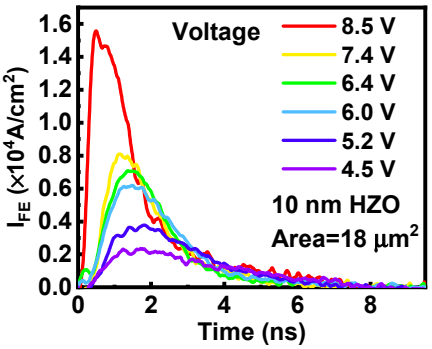

Fig. 15. Transient polarization switching current of 10 nm HZO capacitors under different electric fields.

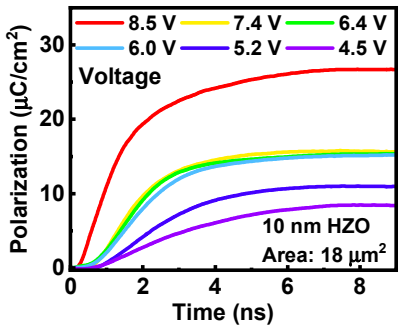

Fig. 16. The corresponding transient polarization charge density from Fig. 15.

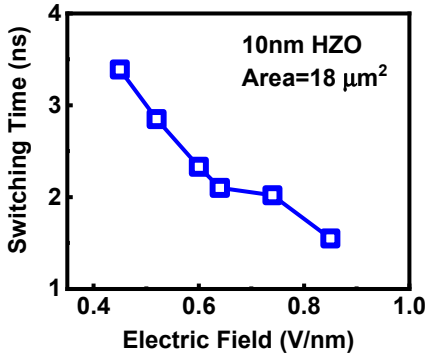

Fig. 17. Electric field dependence of characteristic switching time in 10 nm HZO.

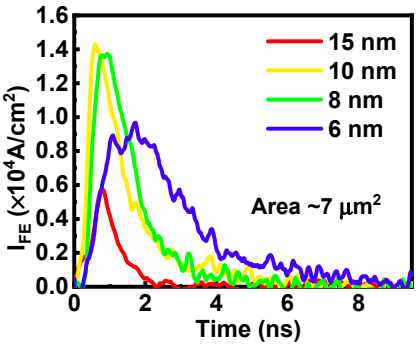

Fig. 18. Transient polarization switching current of HZO capacitors with different thicknesses.

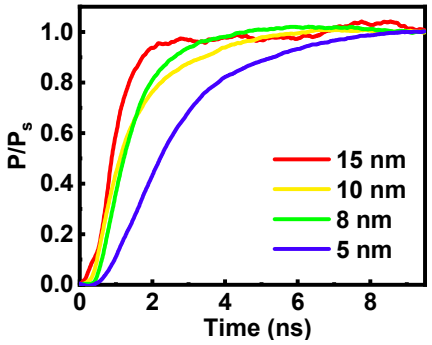

Fig. 19. The corresponding transient polarization charge density from Fig. 18.

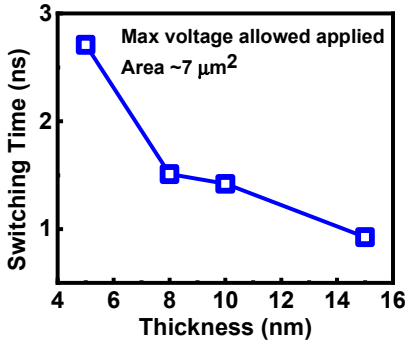

Fig. 20. Fastest characteristic switching time measured in different thicknesses.

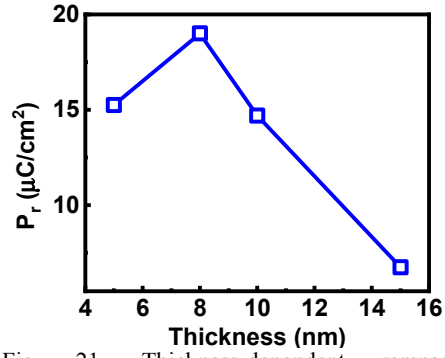

Fig. 21. Thickness-dependent remnant polarization of the HZO capacitor in this work.

	This work Purdue	Ref. 7 Purdue	Ref. 1 Purdue	Ref. 2	Ref. 3	Ref. 4	Ref. 5
Switching Time (ns)	0.925	5.4	3.6	10	100	10	236
FE Oxide Material	HZO	HZO	HZO	Si:HfO_2	Si:HfO_2	Fe-HK	HZO
Thickness (nm)	15	15	10	9	8	/	8
Structure	MIM	MIM	Ge FeFET	Si FeFET	MIM	Si FeFET	MIM
Electrode Material	W	WN	Ni	TiN	TiN	/	W
Voltage (V)	9	6.7	10	6.5	3	4.2	2.5

Table I. Benchmark of FE HfO_2 switching time on MIM and FeFET structures. Sub-ns ferroelectric polarization switching is demonstrated on FE HfO_2 for the first time.

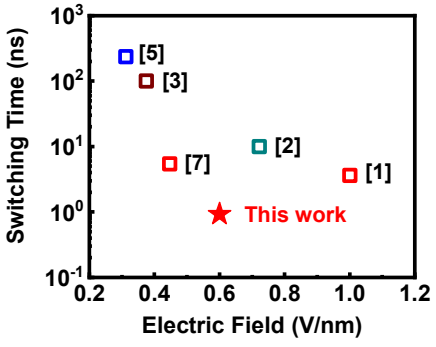

Fig. 22. Benchmark of switching time of FE HfO_2 films versus electric field from reported fastest FE switching speed for both MIM and FeFET structures in literatures.